Multi-objective Optimization of a Solar Assisted 1st and 2nd Generation Sugarcane Ethanol Production Plant

A.S. Wallerand [a*], ***J. Q. Albarelli*** [a], ***A.V. Ensinas*** [a,b], ***G. Ambrosetti*** [c], ***A. Mian*** [a], ***F. Maréchal*** [a]

[a] *École Polytechnique Fédéral de Lausanne, STI-IGM-IPESE, Station 9, 1015 Lausanne, Switzerland*
[b] *Universidade Federal do ABC, CECS, Av. dos Estados 5001, Bloco B 7° Andar, CEP 09210-580, Santo Andre, Brazil*
[c] *Airlight Energy Holding SA, Via Industria 10, 6710 Biasca, Switzerland*
[*] *anna.wallerand@epfl.ch*

Abstract:
Ethanol production sites utilizing sugarcane as feedstock are usually located in regions with high land availability and decent solar radiation. This offers the opportunity to cover parts of the process energy demand with concentrated solar power (CSP) and thereby increase the fuel production and carbon conversion efficiency. A plant is examined that produces 1st and 2nd generation ethanol by fermentation of sugars (from sugarcane) and enzymatic hydrolysis of the lignocellulosic residues (bagasse), respectively. Enzymatic hydrolysis is a promising alternative for 2nd generation biofuels due to its high conversion efficiency and low environmental impact. In conventional ethanol production processes, electrical and thermal power is delivered to the system by burning parts of the feedstock to drive a steam based cogeneration cycle (between 400 and 800K). Introducing high temperature thermal power (at 800K) from a solar trough field coupled with sensible heat storage, for continuous operation, offers the opportunity to replace the heat generated from biomass burning, and thus increase the product yield. In this work, the potential for process integration of a solar trough field coupled with packed bed thermal storage to a 1st and 2nd generation ethanol production site is evaluated by means of pinch analysis. Decision parameters such as the solar fraction, the percentage of bagasse to 2nd generation, and the solar field size are optimized via multi-objective optimization based on evolutionary algorithms to maximize the carbon conversion efficiency and minimize the total annual cost for a plant located in Ribeirão Preto, Brazil.

Keywords:
Solar heat, concentrated solar power (CSP), enzymatic hydrolysis, organosolv lignin, biomass, bioethanol, pinch analysis, process integration.

1. Introduction

The conversion of biomass to ethanol is a promising route with respect to sustainable and carbon neutral fuel production [1]. Utilizing lignocellulosic feedstock such as sugarcane for bioethanol production imposes benefits due to the large production scales, proven conversion technologies, and desirable fuel properties [2]. Sugarcane is commonly converted by fermentation of sugars contained in the juice leading to 1st generation ethanol with bagasse as solid residue. Ensinas et al. [3] show by means of process integration and optimization the potential for higher conversion efficiencies and improved land use by integrating 2nd generation ethanol production through enzymatic hydrolysis of the bagasse (solid residue). There is, however, a bottleneck in the 2nd generation production. The total biomass conversion potential is limited by the process' heat demand, which is nowadays covered by burning the sugarcane leaves and parts of bagasse.
One way to overcome this constraint is by integrating high temperature solar process heat. Mian et al. [4] studied the options for solar thermal power integration to hydrothermal gasification of biomass through process integration and multi-objective optimization of the yearly output based on hourly weather data. The model accounts for variable efficiency of the solar collectors due to low radiation

and varying solar inclination, but does not inlcude a detailed analysis of the piping system and the related optimal size of the solar field. Fixed piping heat losses are considered.
Montes et al. [5] discuss optimization of the solar multiple of a solar-only thermal power plant taking into account the field configuration, but disregard the option of storage and hybridization. They systematically explore the search domain which limits the amount of solutions, while in this paper optimization will be performed by means of an evolutionary algorithm that explores the search space in a randomized manner.
In this work, integration of a novel solar trough concept [6] to a 1^{st} and 2^{nd} generation ethanol production plant similar to the one described by Ensinas et al. [3] is investigated and optimized with respect to thermodynamic, environmental, and economic considerations by application of a methodology making use of process integration techniques and optimization strategies. The solar field is described in a modular fashion with the option to integrate a thermal storage, a conversion unit for the heat transfer fluid (air to steam), and a Rankine cycle. Piping cost and heat losses are accounted for. The investigated objectives are the minimization of the total annual cost (investment and operation) and maximization of the product yield which are both expected to increase with a larger solar field.

2. Methodology

One challenge of this work is to satisfy constant utility requirements imposed the ethanol process with variable solar irradiance. The optimization is performed in two steps. In the master level an initial design configuration assuming constant solar heat supply over the whole year is chosen in a first step. Following that initial decision, energy integration is performed by heat cascading over all available utility and process streams of the ethanol plant including the hot stream from the solar field. This step is referred to as the slave optimization level, which minimizes the operating cost of the system. The energy integration follows an approach by Papoulias and Grossmann [7–9], further developed by Maréchal and Kalitventzeff [10] employing Pinch analysis and heat cascading solved by Mixed Integer Linear Programming (MILP).
The results from the slave optimization are evaluated in the master level. The transience in solar radiation is accounted for by modeling the hourly amount of heat coming from the collectors and the amount that is sent to / coming from the storage unit (if one exists) and / or the amount of heat that has to be provided by a back-up burner. The solar energy balance is closed and the investment costs are derived according to correlations from the literature [11, 12] based on the equipment sizing from the slave optimization and the solar field configuration. The master level optimization is performed with an evolutionary algorithm that produces a Pareto frontier presenting the pareto-optimal equilibria between the two objective functions - the total annual cost and the overall product yield.
The ethanol plant was designed by a detailed flowsheet model in ASPEN PLUS [13] in order to compute the mass and energy balance of the sugarcane biorefinery producing 1^{st} and 2^{nd} generation ethanol and surplus electricity. The overall thermo-economic model was solved in MATLAB-based platform OSMOSE developed at École Polytechnique Fédérale de Lausanne in Switzerland [14] using state variables obtained in the detailed simulation of all equipment and conversion steps of the process.

3. Process description

A superstructure of the ethanol plant together with the solar field is depicted in Figure 1. The ethanol process is supplied with a constant massflow rate of sugarcane and leaves over a certain amount of months (harvest season: from April to November). After the juice extraction, part of the bagasse is fed to the 2^{nd} generation ethanol production while the other part is supplied to the cogeneration system (boiler and steam cycle) in order to provide the system heat requirements. Adding a solar field to the problem enables the use of a larger quantity of bagasse in the 2^{nd} generation ethanol production, although part of it is provided to the solar field back-up burner. Another challenge is the operation of

the solar field during off-season.
The solar field is composed of directly irradiated trough collectors, which are fed with air as heat transfer fluid (HTF). This allows the temperature at the collector outlet to reach as high as 650°C. Three options for providing solar heat to the ethanol system are considered:

- (A) Direct integration - of hot air as HTF from the collectors / storage units to the ethanol process
- (B) Indirect integration - of high temperature steam generated in a heat exchanger placed in the solar field
- (C) Indirect integration - of low temperature steam extracted from a Rankine cycle placed in the solar field

The two last options imply additional investment cost, but at the same time smaller piping losses and, in the case of the latter, efficient electricity production during off-season operation.

3.1. Solar heat

3.1.1. Trough collector and radiation data

The present model of the 1-axis tracking trough collectors is based on a novel series of collectors produced by Airlight Energy Holding SA [6]. They are constructed from a robust and low cost concrete structure supporting reflective polymer films enclosed within an inflated transparent ETFE cushion. By regulation of the pressure difference between the respective foils, an almost parabolic mirror profile is reached.
The solar collector model is based on the physical restrictions of the collector, the optical properties of the foils, the conductive and radiative heat losses of the receiver, and the solar declination angle.

$$P_{\text{coll}} = \eta_{\text{opt}} \cdot \eta_{\text{th}} \cdot f_{\text{a}} \cdot \cos(\theta_{\text{skew}}) \cdot \text{A}_{\text{coll}} \cdot \delta_{\psi} \cdot I_{\text{n}} - \Delta_{\text{l}} \cdot \text{l}_{\text{coll}} \tag{1}$$

with

$$\eta_{\text{opt}}, f_{\text{a}} = f(\theta_{\text{skew}})$$

$$\eta_{\text{th}} = f(\theta_{\text{skew}}, \text{DNI})$$

$$\delta_{\psi} = \begin{cases} 1 & , |\psi| \leq 70^{\circ} \\ 0 & , |\psi| > 70^{\circ} \end{cases}$$

Where $\eta_{\text{opt}} \in [0.5, 0.8]$ is the optical efficiency and $f_{\text{a}} \in [0.9, 1]$ is a correction for the collector's finite length and both are a function of the skew angle θ_{skew}, which is the relative inclination of the sun rays towards the mirror; $\eta_{\text{th}} \in [0.7, 0.95]$ is the thermal efficiency of the receiver as a function of the skew angle and the direct normal radiation (DNI); $\text{A}_{\text{coll}} = 2053$ m^2 is the collector active surface area; δ is a factor accounting for the tracking limits of the collector tracking angle ψ; I_{n} is the direct normal incidence; $\Delta_{\text{l}} = 0.5$ kW/m are the thermal losses per unit length of the receiver hot ducting; and l_{coll} is the collector length.
Figure 2 shows the monthly average of the total daily thermal collector output of a site positioned in Ribeirão Preto, Brasil. The results were generated from DNI data of minute time resolution, which was acquired from a commercial software (Meteonorm 7.0 [15]) based on satellite and ground measurement data using statistical algorithms in order to generate minute resolution. Consequently, this data is not as reliable as measured data, but it is sufficient for estimation of the order of magnitude. According to the software, the yearly DNI in Ribeirão Preto, Brasil, is 1536 kWh/m^2 corresponding to an average of 8.64 MWh/day per collector surface area. The overall yearly thermal efficiency for north-south orientation of one collector is $\eta_{\text{DNI}} = 37\%$ with respect to the DNI. Investigation of

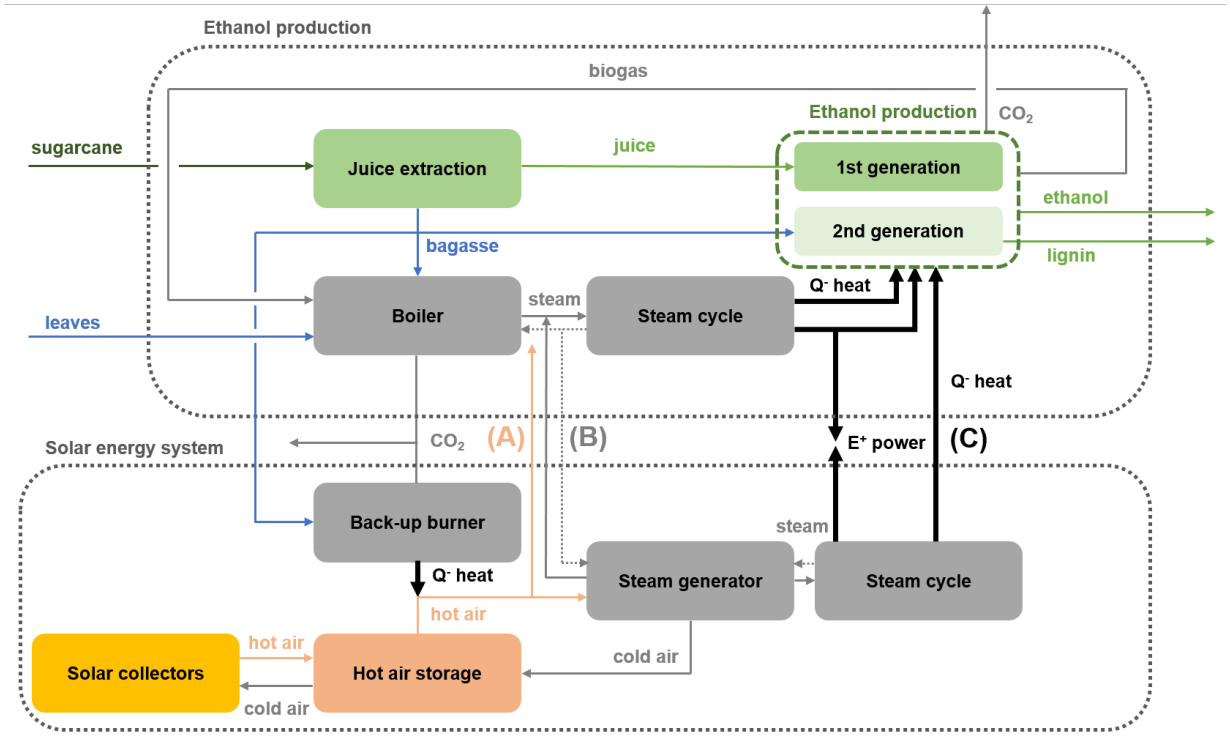

Fig. 1: Superstructure of 1st and 2nd generation ethanol production and solar field with the options of (A) hot air, (B) high temperature steam, and (C) low temperature steam injection to ethanol production.

another source for DNI data based on satellite imagery (Solar Gis [16], 1802 kWh/m^2) shows that the underlying number may be a conservative estimate. Therefore, the solar field might in reality lead to higher thermal output. In any case it is recommended to perform site specific measurements before taking economic decisions. Transient losses (due to the thermal inertia of the system) are not accounted in the present model, as the back-up burner is supposed to compensate for that.
Evaluation of the yearly efficiency and collector output performance was computed on a minute-by-minute basis with help of the Solar Position Algorithm (SPA) published by the National Renewable Energy Laboratory (NREL) [17]. To reduce computation time, the multi-objective optimization was performed with hourly averages of the minute-by-minute collector output data.

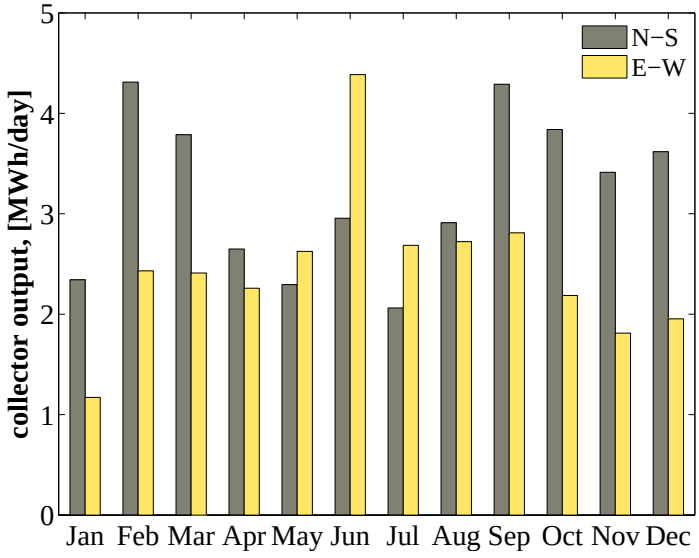

Fig. 2: Monthly average of daily solar collector output for a site positioned in Ribeirão Preto, Brasil, -21.1°N, -47.48°E, solar irradiation data from [15], yearly DNI 1536 kWh/m^2.

3.1.2. Solar field model

The solar field is structured in a modular form in order to quantify the influence of the piping system on the overall performance with respect to losses and cost. Figure 3 depicts the general setting of the field. In Table 1 parameters used for calculating the field performance are depicted.
The smallest unit {*Level 1*} is composed of two collectors in a row ($N_{1,tot} = 2N_1 = 2$) . The connecting pipes towards the next level are positioned in between the two collectors. The second level alignes several level 1 units along one joining pipe ($N_{2,tot} = 2N_2 \cdot N_{1,tot}$). The connection towards the next level or the ethanol plant is attached in the middle. The third level alignes several level 2 units along one joining pipe ($N_{3,tot} = 2N_3 \cdot N_{2,tot}$) and so on.

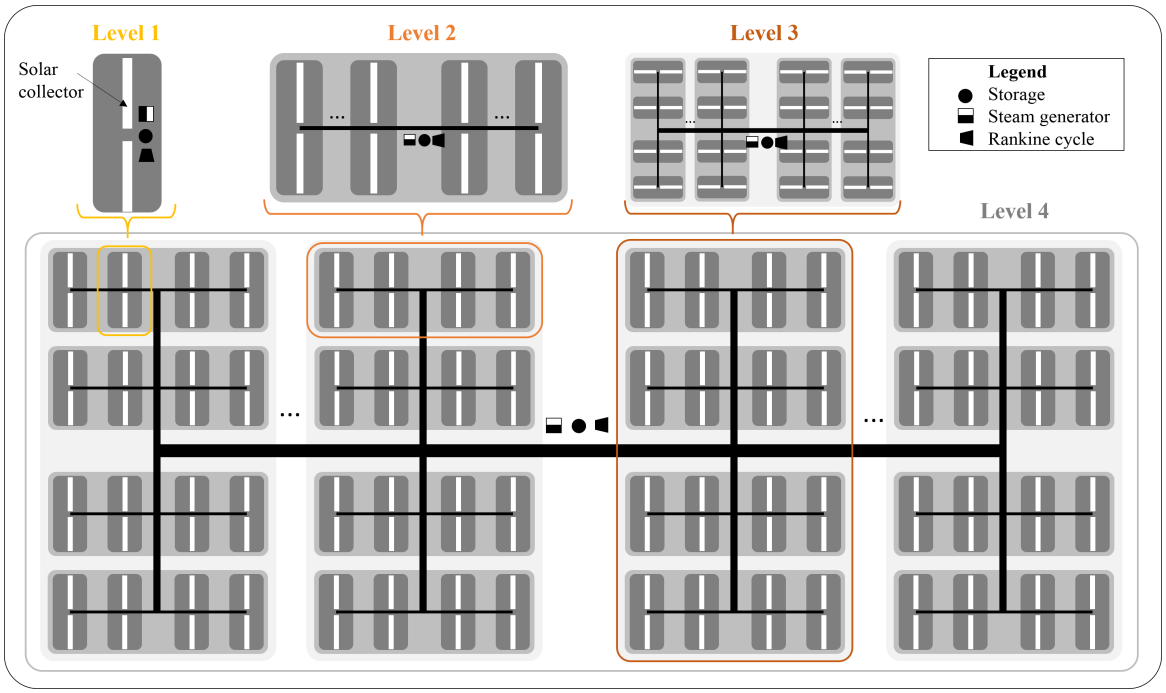

Fig. 3: Modular solar field configuration with optional storage units, steam generators and Rankine cycles.

The piping heat losses and the cost estimation are based on the length and the diameters of the pipes. The diameter of a duct connecting N_x elements is calculated based on the mean cross-sectional area which depends on the heat transfer fluid (HTF) maximum velocity, the density, and the maximum mass flow rate in the duct, which depends on the number of elements.

$$d_{x,mean} = 2 \cdot \left(\frac{A_{x,mean}}{\pi} \right)^{\frac{1}{2}} \tag{2}$$

with

$$A_{x,mean}(N_x) = \frac{N_x + 1}{2} \cdot \frac{\dot{m}_{x-1} \cdot \mathrm{R} \cdot \mathrm{T_{ht}}}{\mathrm{v_{ht}} \cdot \mathrm{p}}$$

Where $\dot{m}_{x-1} = N_{x-1,tot} \cdot \dot{\mathrm{m}}_{\mathrm{max,coll}}$ is the mass flow rate leaving from the previous level, R is the mass based gas constant, $\mathrm{T_{ht}}$ is the high temperature of the heat transfer fluid and p is the pressure inside the pipe.
As each level consists of two strings of attached elements, the length of the piping in a specific level is calculated by doubling the length of one string.

$$l_x = 2 \cdot N_x \cdot w_x \tag{3}$$

with

$$w_x = l_{x-1}$$

The initial width of an element is given by the minimum spacing distance (w_1 = 35m) developed from the tracking limit and the initial length of an element, which is given by twice the collector length ($1_1 = 2 \cdot 211.6$m).
The cost estimation for the hot air and steam pipes is based on the assumed market price of steel pipes of 250 \$/t [18]. Assuming a steel density of 7.8 t/m^3, a diameter of 2.5 m, and a pipe thickness of 15 cm, this leads to approximately 2'500 \$/$m_{\text{hot duct}}$. Calculated piping diameters above 3m are separated into several pipes with same total cross-sectional area.
The piping heat losses are derived according to the formula given below.

$$h_{wall} = \frac{1}{\frac{r_o}{h_i \cdot r_i} + r_o \cdot \sum_m \frac{\ln(r_{m+1}/r_m)}{k_m} + \frac{1}{h_o}} \tag{4}$$

Where r_i, r_o, and r_m are the pipe's inner radius, outer radius, and the radius up to the respective insulation shield layer; h_i, h_i, and k_m are the inner, outer convective heat transfer coefficient, and the thermal conductivity of each layer. In agreement with [11] the pipe's inner convective heat transfer coefficient, h_i, is not the limiting resistance and can therefore be neglected. The pipe insulation is envisioned to be a multi-shield build of layers of aluminum foil and air. The average heat losses are computed assuming 20 levels of air and aluminum, a pipe diameter of 2m, and a temperature difference towards the surrounding of 550K.
The storage is envisioned as a packed bed of rocks [19] and its operating range is defined by the solar multiple, sm, or solar fraction, f_{sm} at the design point. The solar fraction manifests the fraction of the solar collector output which is is directly used while the rest ($1 - f_{\text{sm}}$ at design conditions) is sent to the storage.

$$f_{\text{sm}} = \frac{1}{\text{sm}} = \frac{\dot{Q}_{th\ \text{air to ethanol process}}}{\dot{Q}_{th\ \text{solar collector out, design}}} \tag{5}$$

The rate at which the storage is emptied or filled depends on the actual solar output.

$$\dot{Q}_{n,\ \text{stor}} = \begin{cases} \dot{r}_{n,\ \text{stor}} & , \delta_{n,\ \text{stor}} \geq 0 \\ \sum_{n-1} \dot{Q}_{n-1,\ \text{stor}} \cdot \eta_{\text{stor}} & , \delta_{n,\ \text{stor}} < 0 \end{cases} \tag{6}$$

with

$$\delta_{n,stor} = \sum_{n-1} \dot{Q}_{n-1,\ \text{stor}} \cdot \eta_{\text{stor}} + \dot{r}_{n,th\ \text{stor}}$$

$$\dot{r}_{n,th\ \text{stor}} = \dot{Q}_{th\ \text{solar collector out}} - f_{\text{sm}} \cdot \dot{Q}_{th\ \text{air to ethanol process}}$$

The first row of equation 6 describes the case, when the storage is either filled or emptied, making sure that the ethanol process is supplied with the constant requirement, $\dot{Q}_{th\ \text{to ethanol}}$. In the second case, the storage content is not enough to cover for the full ethanol process heat requirements and is, thus, completely emptied. During production season, the back-up burner covers the lack of thermal power delivered from the sun and storage. During off-season the solar heat is fully converted to electricity, with help of the steam generator and Rankine cycle contained in the solar field or (if not present in the solar field) in the ethanol plant. In the latter case part load efficiency reduction of the Rankine cycle is accounted for by the correlation suggested by Augsburger [20] and it is asumed that the ethanol steam generator heat transfer efficiency is only 50% at part load. Still, this assumption is simplified and needs more thorough investigation at a proceeding stage. In that time, the back-up burner is not used as no bagasse is harvested. It is assumed the the solar back-up burner has a lower efficiency (95%) than the ethanol boiler, as it is supposed to be more flexible and operate in a wide range.
The cost for the thermal storage system was taken from Fricker et al.'s [21] evaluation of a packed bed storage streamed with air by, who's system operates at a similar temperature range. However, as they clearly state, 2/3 of the cost arise from the high costing steel container, and in this study only

low-cost concrete is considered. Thus, the specific cost was adjusted by a factor of 1/3, leading to 7 \$/kWh$_{th}$. Regarding the solar collectors, the cost assumption was taken from Langnickel et al. [22]. The operating temperature range in this study is higher than that in Langnickel's and therefore the price was doubled, resulting in ca. 500 \$/m$^2_{\text{active surface}}$.

Table 1: Parameters of the solar field.

Parameter	Symbol	Value	Unit	Ref
Solar collector length	l_{coll}	211.6	m	[6]
Solar collector width	w_{coll}	9.7	m	[6]
Solar collector surface area	A_{coll}	2053	m^2	[6]
Minimum parallel collector spacing	w_1	35	m	calc.
Collector maximum power output (DNI 1000 W/m^2)	$\dot{Q}_{max,coll}$	1360	kW	calc.
Collector maximum air mass flow rate	$\dot{m}_{max,coll}$	2.4	kg/s	calc.
Yearly DNI	DNI	1536	kWh/m^2	[15]
Collector yearly efficiency	η_{DNI}	37	%	calc.
High temperature air velocity	$v_{ht\ air}$	40	m/s	[23]
High temperature steam velocity	$v_{ht\ steam}$	50	m/s	[23]
Piping high temperature heat losses per surface area	$\Delta_{ht,pipe}$	0.19	kW/m^2	calc.
Piping low temperature heat losses per surface area	$\Delta_{lt,pipe}$	$0.19\frac{T_{lt}-T_o}{T_{ht}-T_o}$	kW/m^2	calc.
Thermal conductivity of aluminum	k_{al}	0.237	kW/mK	
Thermal conductivity of air (800 K)	$k_{ht\ air}$	577e-7	kW/mK	
Aluminum layer thickness	d_{al}	0.05	mm	
Air layer thickness	d_{air}	10	mm	
Outside convective heat transfer coefficient	h_o	15	kW/m^{2}K	[11]
Efficiency of back-up burner	η_{burner}	81	%	calc.
Efficiency of steam generator	η_{sg}	88	%	calc.
Thermal efficiency of Rankine cycle	$\eta_{Rank,th}$	76	%	calc.
Electrical efficiency of Rankine cycle	η_{el}	24	%	calc.
Electrical efficiency of Rankine cycle (off-season)	$\eta_{el,off}$	25	%	calc.
Storage losses over 24h	$(1-\eta_{stor})\cdot 24$	2	%	[19]
Air collector outlet temperature (1 bar)	$T_{ht\ air}$	650	C	[6]
Air collector inlet temperature	$T_{lt\ air}$	120	C	[6]
Steam generator outlet temperature, 90 bar	$T_{ht\ steam}$	503	C	calc.
Steam generator inlet temperature, 0.12 bar	$T_{cond\ steam}$	50	C	calc.
Rankine outlet temperature, 2.2 bar	$T_{lt\ steam}$	125	C	calc.

3.2. Ethanol plant

3.2.1. Integrated ethanol production

The simulation of the sugarcane biorefinery producing 1st and 2nd generation ethanol and electricity was fully described in detail elsewhere [3, 24] except from the organosolv pretreatment used in the underlying study. The biorefinery is dedicated to the production of anhydrous ethanol with 99.3% (w/w) of purity, which is the specification for blending with automotive gasoline. Figure 4 shows the diagram of the sugarcane biorefinery producing ethanol, lignin and electricity. The first generation ethanol production process is evaluated considering technologies available in modern ethanol distilleries in Brazil, including sugarcane dry cleaning, concentration in multi-effect evaporators, sterilization of the juice before entering the fermentation system and ethanol dehydration using Monoethylene Glycol (MEG). Sugarcane bagasse is considered for saccharification through three major steps: preparation, pretreatment and hydrolysis.

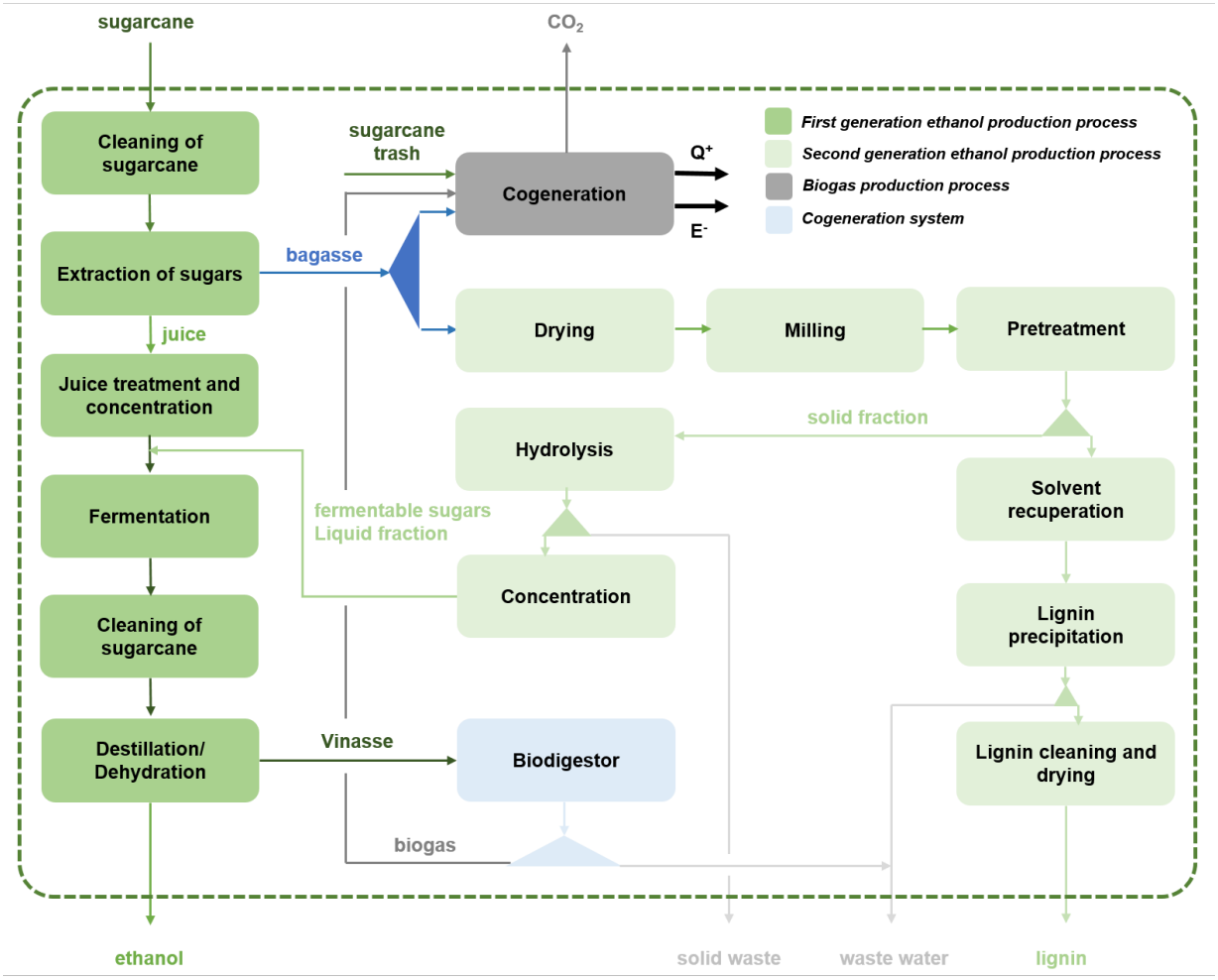

Fig. 4: Superstructure of 1st and 2nd generation ethanol production.

In the preparation unit, bagasse, derived from the juice extraction process with 50% of moisture, is dried with hot air (100°C) until 8% (wt.) moisture content (equilibrium moisture of bagasse at temperatures around 25°C and atmospheric pressure) and milled.

In the pretreatment step, bagasse is treated by organosolv pretreatment, at 180°C, which consists of: the lignin removal (73%), the hemicelluloses hydrolysis to xylose (56.7%) and acetic acid (56.2%), the degradation of xylose to furfural (7.3%), and the hydrolysis of cellulose to glucose (12%). Product yields for the pre-treatment reactor are calculated using data from Pan et al. [25].

After the pre-treatment, the pulp is washed with solvent and water to remove lignin and contaminants. The enzymatic hydrolysis is conducted at a temperature of 45°C with a solid load of 2%, residence time of 24h and enzyme loading of 27 mg of enzyme/g of cellulose. All data for simulation of the pretreatment and hydrolysis step are based on the experimental results of reference [25]. Although Pan et al. evaluated organosolv pretreatment for poplar wood, the same parameters are used for bagasse based on the knowledge that this pretreatment produces very similar results for different biomasses [26].

After the hydrolysis reactor, a concentration of the produced hydrolysate is carried out in an evaporator with four effects. The concentrated hydrolysate is then sent to the 1st generation process plant where it is mixed to the concentrated juice and then sent to fermentation. The liquid stream from the pretreatment is sent to a solvent recovery step with 2 columns working in parallel at different pressures (1 bar and 4.5 bar). After solvent recovery, water is added to the lignin rich liquor, 3 parts of water to 1 of liquor (w/w). Lignin precipitation occurs, it is separated from the liquid stream by centrifugation, cleaned with water and dried. Residual water is sent to the water treatment facility and reused in the process. The residual vinasse is used to biogas production through anaerobic digestion. The production of biogas is assumed to take place in an UASB biodigestor operating at 30 °C. The

biodigestor was simulated as a stoichiometric reactor where the organic matter decompositions to methane and carbon. The reaction yield of the production of methane from biomass in the reactor is estimated to be 70%.
Main process parameters considered for the simulation and the sugarcane composition entering the process are displayed in Table 2 and 3.

Table 2: Parameters for 1st and 2nd generation ethanol production.

Parameter	**Value**	**Unit**
Sugarcane processed	500	t/h
Production season (Apr-Nov)	210	days
Preparation and sugarcane juice extraction		
Efficiency of dirt removal on sugarcane cleaning	60	%
Efficiency of sugars extraction on the mills	97	%
Sugarcane bagasse moisture content	50	%wt
Juice treatment		
Recovery of sugars on juice treatment	99.4	%
Bagasse pretreatment		
Organosolv pretreatment time	60	min
Solvent (ethanol) - water ratio	1:1	
Lignin removal from pretreated solid	73	%
Hydrolysis		
Enzymatic hydrolysis	24	h
Cellulose conversion to sugar	93	%
Lignin recovery		
Lignin final solid product recovered after pretreatment	55	%
Fermentation		
Fermentation yield	89	%
Ethanol recovery		
Ethanol recovery on distillation and dehydration	99.7	%

Table 3: Sugarcane stalk and leaves composition.

		Stalk % wt	**Leaves** % wt
Water		70.5	15
Fibers	Cellulose	5.9	35.7
	Hemicelluloses	3.5	28.1
	Lignin	3.2	19.8
Solids	Sucrose	13.9	–
	Dextrose	0.6	–
	K2O	0.4	–
	KCl	0.2	–
	SiO2	0.3	–
	Acronitic acid	0.6	–
Impurities	SiO2	1	1.4
LHV (MJ/kg)		7.5	14

3.2.2. Cogeneration system

The fuels considered for the cogeneration system are: sugarcane leaves, biogas produced from vinasse and parts of the bagasse. The burner heat conversion efficiency is approximately 90%. The amount of bagasse used at the cogeneration system varies according to the studied scenario. A saving of 10% of bagasse is assumed with the purpose of having a back-up fuel during the cogeneration startup or sugarcane crushing shutdowns. The flow of sugarcane-leaves is calculated considering that 40% of this material produced at the harvest is collected and used for cogeneration, this represents a flow of 33 t/h. Composition of leaves material considered for simulation is shown in Table 3.
A Rankine cycle cogeneration system is used to supply heat and power to the process. Steam at 503°C and 90 bar is considered and steam turbines with extractions at several pressure levels are simulated. The entire cogeneration system is integrated with the process when the heat cascade problem is solved.

3.3. Performance indicators

The evaluated performance indicators are the yearly global efficiency η_{GHI}, the total annual cost I_{tac}, which stems from the annualized investment cost and the operating cost, and the carbon fixation rate C_{fix}. The underlying economic parameters are displayed in Table 4. The global efficiency is derived from the ratio between the yearly energy produced and the total available solar radiation (global horizontal radiation - *GHI*) present on the ethanol field. The yearly energy produced is a sum over all products multiplied by their lower heating value and the net generated electricity. The net generated electricity is divided by the combined cycle heat-to-electricity efficiency (η_{CC} = 55%) in order to calculate thermal equivalent energy of electricity. The global efficiency is defined as follows.

$$\eta_{GHI} = \frac{LHV_{\text{products}} \cdot m_{\text{products}} + \frac{\Delta E_{el}}{\eta_{CC}}}{GHI \cdot \text{A}_{\text{sugarcane field}}} \tag{7}$$

As the ethanol process delivers ethanol and high quality lignin, the carbon fixation rate is defined for valorizing the process' product yield and especially the carbon capture potential. The produced green electricity is not taken into account as a positive influence. However, during the optimization, the electricity balance was not allowed to be negative such that imported non-green electricity could not positively bias the carbon fixation rate.

$$C_{0,fix} = \frac{\text{mols of carbon in lignin and ethanol}}{\text{mols of carbon in sugarcane and leaves}} \tag{8}$$

The carbon fixation rate is normalized by the land surface area. This is done in order to take into account that the solar field partly inhibits sugarcane planting and harvesting. The correction factor f_{area}, forms to

$$f_{area} = \frac{\text{A}_{\text{sugarcane field}}}{\text{A}_{\text{sugarcane field}} + A_{solar}}$$

and

$$C_{fix} = C_{0,fix} \cdot f_{area}$$

Where the solar area is estimated by the product between the total amount of collectors times active surface area times a safety factor to account for partial shadowing of the crops: $A_{solar} = N_{tot} \cdot \text{A}_{\text{coll}} \cdot 1.2$. The economic study is undertaken considering fixed capital cost, production cost, and revenues. The formula for calculating the total annual cost is derived by annualization of the investments, I_{inv}, the operational expenses due to raw material cost, $C_{\text{raw material}}$, the maintenance cost, M, as well as net electricity cost, ΔE_{el} .

$$I_{tac} = \frac{\text{i} \cdot (\text{i}+1)^{\text{lt}}}{(\text{i}+1)^{\text{lt}} - 1} \cdot I_{inv} + \sum C_{\text{raw material}} + \Delta E_{el} + M \tag{9}$$

The annual benefits are not accounted in the total annual cost in order to keep the cost independent from the product yield. The process equipment is sized and the purchase cost is calculated and adjusted to account for specific process pressures and materials using correlations from the literature [11, 12]. The total investment cost is then calculated by using multiplication factors to take into account indirect expenses like labor, transportation, fees, contingencies and auxiliary facilities. The operating cost take into account the cost of labor, maintenance (5% of the total investment), the main raw materials (sugarcane, sugarcane leaves, enzymes), and extra utilities (electricity), if the cogeneration system does not generate sufficiently. The total yearly cost is the sum of the operating cost and the depreciation cost, the latter being the total investment cost divided by the present worth of annuity. All costs have been updated to the year 2012 by using the Marshall and Swift Index.
The decision parameters for the non-linear optimization are the number of levels N_{lev}, the amount of collectors per level N_x, the solar fraction f_{sm}, the fraction of bagasse to 2^{nd} generation ethanol production f_{2g}, the amount of bagasse substracted from the ethanol cogeneration unit to the solar back-up burner(s) f_{2b}, and the solar field level positions of the thermal storage unit p_{stor}, the steam generator p_{sg}, and the Rankine cycle p_{rank}. The ranges of the parameters are depicted in Table 5.

Table 4: Performance indicators

Data	Value	Unit
Project lifetime, *lt*	25	years
Construction and startup	2	years
Depreciation	10	years
Interest rate, *i*	15	% year
Ethanol average price	0.72 [27]	$/l
Electricity average price	51 [27]	$/MWh
Lignin average price	500 [28]	$/t
Days worked in a year	210	days/year

Table 5: Decision parameters

Decision parameters	Range
Bagasse to 2^{nd} generation, $f_{b_{2g}}$	0.4:0.9
Bagasse to burner, $f_{b_{2g}}$	0.1:0.7
Solar fraction, f_{sm}	0.05:0.4
Number of Levels, N_{lev}	1:4
Number of elements in level 2,3,4, N_x	1:20
Position of storage, steam gen., Rankine	0:4
Pressure level 1 (bar)	10:20
Pressure level 2,3,4 (bar)	0.1:10
Pressure level 5 (bar)	0.1:7
Superheating temperature (dK)	100:300

4. Results

Figure 5 shows the hourly heat release from the solar field for the days 118 up to 123 of the year. The data is normalized by the solar collectors' output at design conditions (1360 kW $\cdot N_{tot}$). As the ethanol production season only starts at the end of April ($4 \cdot 30 =$ day 120), the heating rate towards the ethanol plant is only activated after day 120. Before, the heat released from the collectors / storage is converted to electricity (P_{el}^{-}) either in the case of (a,b,c) by means of the steam generator and Rankine cycle contained in the ethanol plant, or by the steam generator and a Rankine cycle contained in the solar field (d). The solar fraction rate (Q_{sm}) manifests the fraction of the design solar collector output which is further processed (sent to ethanol / steam generator), while any collector heat release above this fraction is transferred to the thermal storage.
For this reason, it is evident that with decreasing solar fraction (from (a) to (c)), the thermal storage is loaded more intensely and requires more storage volume. Therefore, the electricity output during off-season (in the period of days shown) is only constant for the solar fraction of 0.1. As the solar field Rankine cycle is sized according to the expected thermal output, the electrical efficiency (d) is distinctly higher than the one resulting from the ethanol plant Rankine cycle (c).
The burner is only activated during ethanol production season as to minimize the feedstock utilization rate. This may be observed in the case of (a) and (b), where the burner is activated as soon as the collector output and the stored heat are not sufficient to deliver constant heat towards the ethanol process after day 120, when the season starts.
In Figure 5 (d) the heating rate towards the process is lower than the one in (c) even though the same solar fraction is assumed. This stems from the existence of a steam generator and Rankine

cycle within the solar field in that scenario which leads to a lower thermal power output due to the respective conversion efficiencies and the electrical power production (the solar fraction is defined for air as heat transfer fluid).

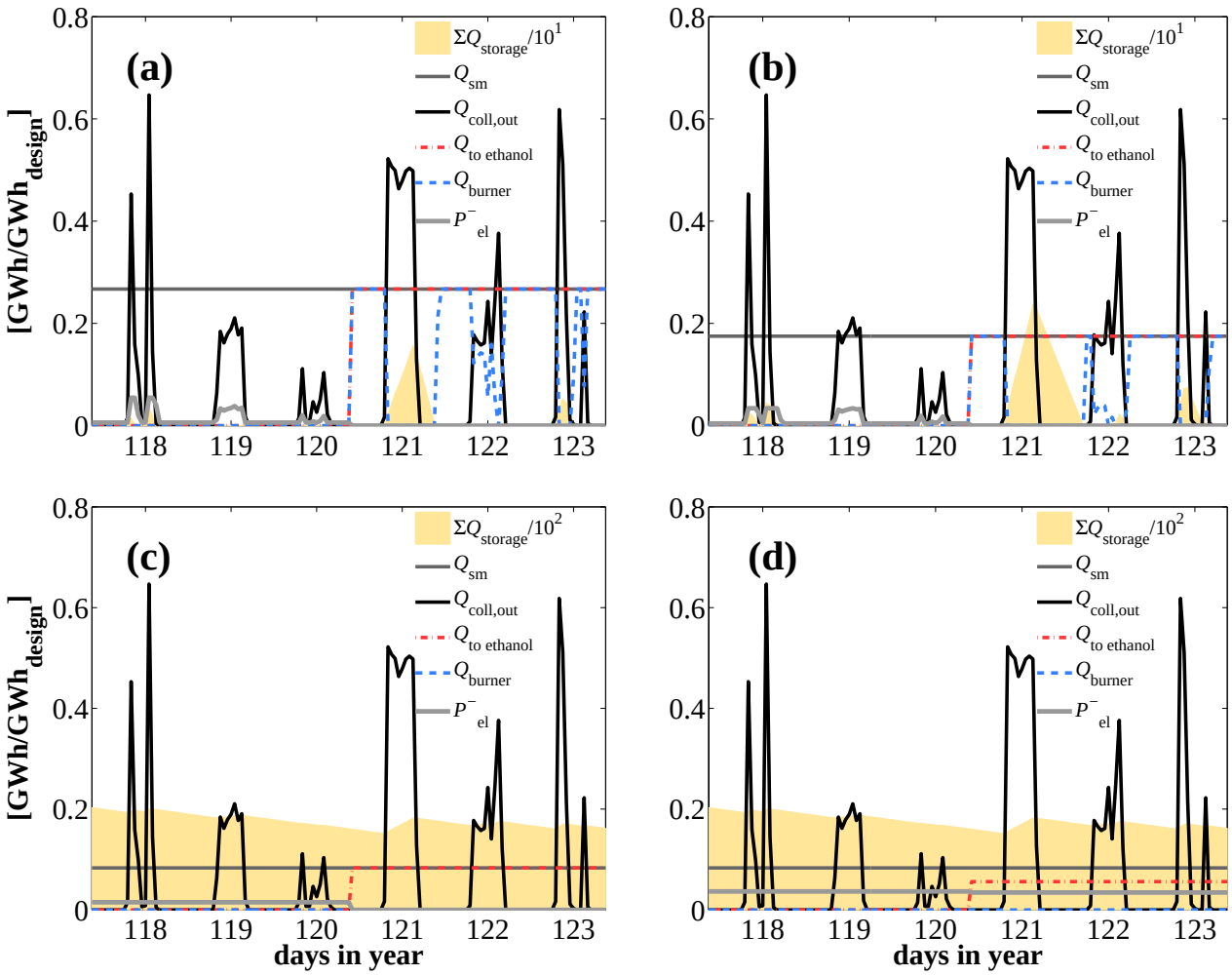

Fig. 5: Hourly energy content of storage, thermal energy output of the collectors and constant heat supplied to the ethanol process, heating requirements by burner, and electricity produced from solar energy, all normalized by the design total thermal output. The field size is 4 levels of $N_1 = 1$, $N_2 = 5$, $N_3 = 5$, and $N_4 = 5$ with a total of $N_{tot} = 2000$ collectors. **(a)** *p_{stor}=1, p_{sg}=1, p_{Rank}=1, $f_{sm} = 0.3$,* **(b)** *same as (a) except $f_{sm} = 0.2$,* **(c)** *same as (a) except $f_{sm} = 0.1$,* **(d)** *same as (c), except p_{stor}=1, p_{sg}=4, p_{Rank}=4. Site positioned in Ribeirão Preto, Brasil, -21.1°N, -47.48°E, [15]*

Figure 6 shows a Pareto frontier between the total annual cost and the product yield manifested in the carbon fixation rate for different solar collector quantities in the solar field. Different points are highlighted (ref I - 1st generation ethanol only, ref II - 1st and 2nd generation ethanol, and (a,b,c,d) - solar integrated 1st and 2nd generation ethanol) that are further discussed in the next section.
The frontier can be separated into a part with higher and with lower gradient. The part with lower gradient between a carbon fixation rate of 0.22 and 0.28 marks the range where there is little to no solar integration but mostly different fractions of 2nd generation ethanol integration to the 1st generation plant. After the threshold of 0.28, which also marks the thermodynamic maximum of 2nd generation integration without external heat sources (such as the sun), the cost increases more distinctly due to higher investment cost caused by the solar field. It can be observed that with increasing numbers of solar collectors the carbon fixation rate and the annual costs increase distinctly. The maximum carbon fixation rate of 0.33 is given by maximum amount of bagasse (90%) that can be sent to the 2nd generation ethanol production. It can be seen that for solar collector quantities around 3000 this limit is reached.

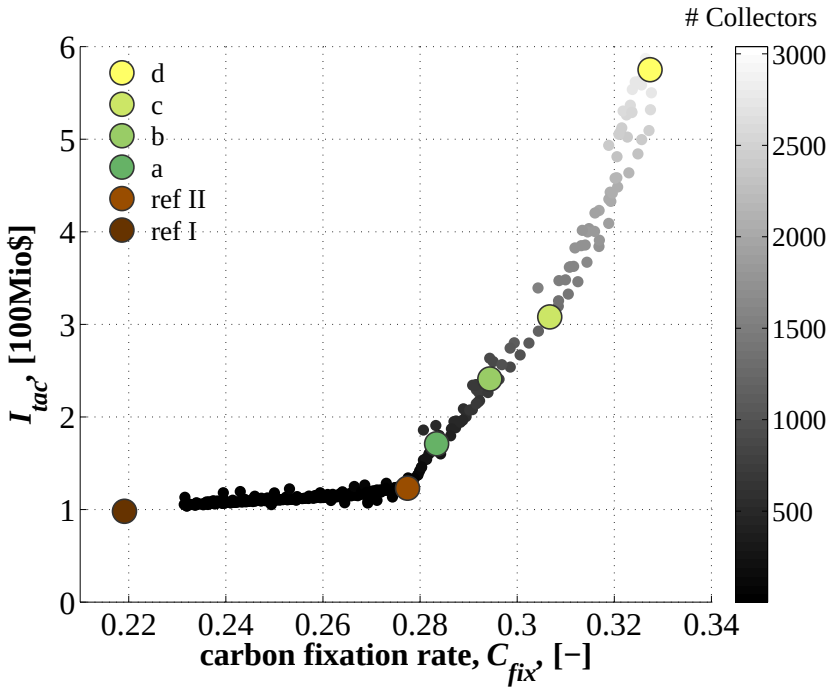

Fig. 6: Pareto curve showing the total annual cost versus the carbon fixation rate for different total collector quantities.

Table 6 displays a detailed record of the points highlighted in the Pareto curve. The first reference (ref I) scenario is the stand-alone 1^{st} generation ethanol production plant. This is further integrated in the second reference scenario (ref II) additionally integrating 2^{nd} generation ethanol production and still being energy wise self-sufficient, by supplying f_{2g} = 45.6% of the total amount of bagasse to the 2^{nd} generation ethanol production and transmitting the remaining available 34.4% to the cogeneration unit (the last 10% are kept as back-up fuel, chapter 3.2.2.).
Scenarios a - d* represent different degrees of solar integration to ref II. The maximum possible carbon conversion rate, scenario d, is determined by sending all available bagasse to the 2^{nd} generation ethanol production. Scenario d* is adapted from d also targeting the maximum possible carbon conversion rate, but additionally increasing the solar heat input to optimize the cogeneration potential by maximizing the steam network integration.
With respect to ref I, the integrated 1^{st} and 2^{nd} generation plant (ref II) imposes higher product yield and therefore more carbon caption per plant surface area and even slightly higher profit. By integration of a solar field (a - d*), the carbon fixation per surface area can be further elevated resulting in lower or even negative profit. Increase of the carbon fixation rate from ref I to ref II stems mainly from a reduction of bagasse feedstock sent to the cogeneration unit with the result of less electricity output. Further increase of the product yield due to solar collectors integration lies in the higher solar-to-thermal conversion efficiency per surface. The yearly efficiency of the solar collectors from incident solar radiation to thermal energy reaches 37% while the photosynthetic efficiency of sugarcane growth lies below 1%.

Figure 7 shows a distribution of the investment cost (I_{inv}) of the scenarios depicted in Table 6 and a detailed cost distribution of the 1^{st} and 2^{nd} generation ethanol production. The 1^{st} generation ethanol production investment is 225 Mio$ which is in the same order of magnitude as values from literature [29]. The largest parts are the utilities (comprising burners, heat exchanger network, and steam turbine), milling, and fermentation. The investment cost of the 2^{nd} generation ethanol production is less than a quarter of the 1^{st} generation plant, the largest part is imposed by the hydrolysis. Investigation of the investment cost distribution (Figure 7 left) shows that the solar field is the predominant factor.

Table 6: Integration scenarios. Ref I - stand-alone 1st generation ethanol production, ref II - integrated 1st and 2nd generation ethanol production, a - d - different scenarios of solar integration to ref II.*

Name	N_{tot} #	C_{fix} -	f_{2g} -	f_{2b} -	f_{sm} -	N_{lev} #	p_{stor} -	p_{sg} -	p_{rank} -	I_{tac} 100 M$	**Benefit** 100 M$	**Profit** 100 M$
ref I	0	0.219	0	0	-	-	-	-	-	0.98	1.43	0.45
ref II	0	0.277	0.456	0	-	-	-	-	-	1.23	1.71	0.48
a	320	0.283	0.508	0.20	0.109	3	3	-	-	1.71	1.74	0.03
b	840	0.294	0.606	0.42	0.113	3	3	2	3	2.41	1.80	-0.61
c	1232	0.307	0.706	0.22	0.095	3	1	-	-	3.08	1.86	-1.22
d	2880	0.327	0.900	0.00	0.081	3	1	-	-	5.75	1.98	-3.77
d*	4000	0.324	0.900	0.00	0.081	3	1	-	-	7.42	1.98	-5.44

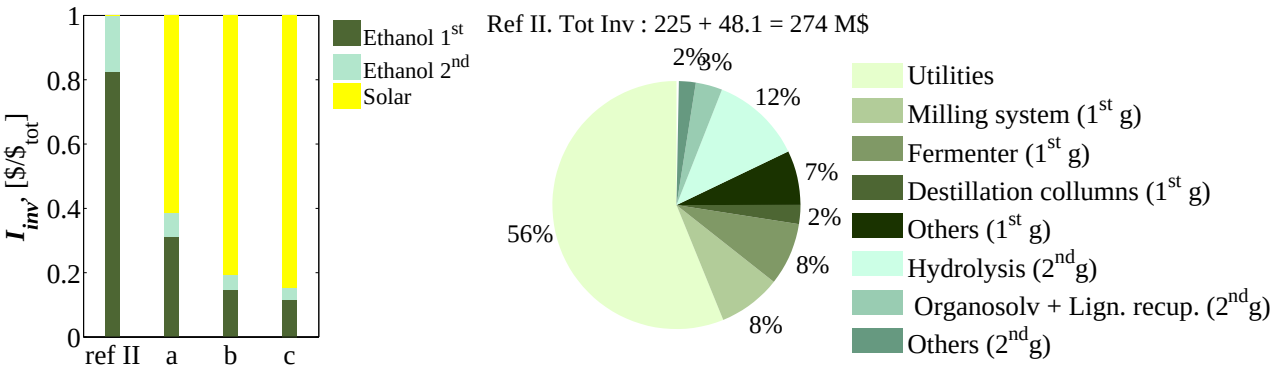

Fig. 7: Left: Normalized distribution of investment cost (I_{inv}) between ref II and different solar field scenarios. Right: Detailed cost distribution of 1st and 2nd generation ethanol production of ref II. (Utilities: Cogeneration system, heat exchanger network, pump system)

Figure 8 shows the investment cost distribution of the solar field for scenario a and b. In scenario a, the solar field is assumed to be composed of pipes, collectors and storage units while in scenario b also steam generators and a Rankine cycles are considered to be installed in the solar field. This means that only low temperature steam is transferred across the field towards the ethanol production. Thus, the piping cost are significantly reduced, while the utility cost are increased. This can be seen in the charts (Fig. 8). In both cases the storage cost is a dominant factor. This is mainly due to the very low solar fractions (f_{sm}) and therefore high storage volumes. The cost assumptions taken here for the storage and collectors are very conservative and leave room to speculation, as the technology is not yet established and a reduction due to economies of scale may be expected.

Figure 9 displays the steam network plotted over the residual streams of scenario ref I and ref II, d and d*. It can be seen that the pressure levels of the turbine draw-offs are well integrated for ref I. The steam network of ref II has a much lower capacity as a high amount of the available exhaust heat from the biomass burners is required to fulfill the additional process needs given by the 2nd generation process. It can also be observed that there is still room for process optimization by heat pumping or pressure level adaption with respect to the 2nd generation distillation columns' (horizontal) streams between 80^oC and 120^oC. That is, however, not included in the scope of this work.
Scenario d and d*, on the right side of Figure 9, show two cases of solar integration. Addition of solar heat accounts for the truncation of the curves between 650^oC and 120^oC and for the offset above 600^oC. It can be seen that the steam network integration and the electricity production in scenario d is only very slightly increased compared to ref II. The additional amount of heat from the solar field is used instead to increase the ethanol production line and with that the product yield. In scenario d* the steam network is best integrated which leads to a distinct increase in electricity production from 59 kW_{el}/MW_{sc} to 169 kW_{el}/MW_{sc}.

Table 7 summarizes the energy balance, product yield, and the solar area fraction of the respective scenarios. The global efficiency of ref I of 0.365% shows the maximum potential of a 1^{st} generation only ethanol production plant by optimal steam and heat exchanger network integration. From ref I to ref II, the maximum efficiency at highest possible product yield decreases, due to a drastic decrease in electricity production caused by a lack of available high temperature heat. By solar integration the global efficiency can be improved up to the last scenario d* by round 40% compared ref I. The reason for the increase of the overall efficiency due to solar integration is the superior solar-to-heat ratio of the solar collectors towards the photosynthesis and with that higher product yield per surface area. This is also the reason, why scenarios with high solar integration still have a low area fraction in contrast to the ethanol field (0.38% for 2880 collectors in scenario d). The high increase in the global efficiency (η_{GHI}) from scenario d to d* results from the optimal integration of the steam network (see Figure 9). Here, the exergetic losses of the system are minimized and by addition of only 135 kW_{th}/MW_{sc} solar heat, supplementary 110 kW_{el}/MW_{sc} electricity is generated which results in an equivalent marginal efficiency from heat to electricity of 80%.

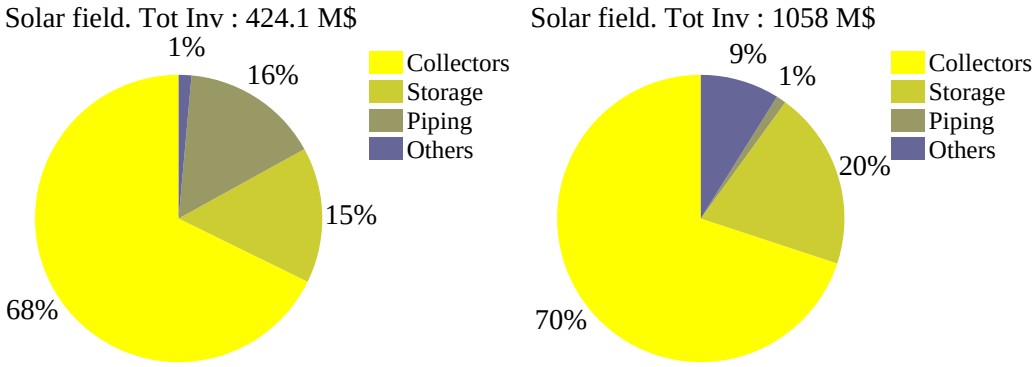

Fig. 8: Investment cost distribution of the solar field for scenario a - left, and b - right. The back-up burner and pump cost are contained in 'Others'.

Table 7: Product yield, net electricity production, solar area fraction, and global efficiency with respect to a yearly GHI of 1741 kWh/m² [15].

	anhydros ethanol kg/h	**lignin** kg/h	$\Delta E_{ethanol}$ GWh/a	ΔE_{solar} GWh/a	$1 - f_{area}$ %	η_{GHI} %
ref I	31116	0	381.2	0.0	0.0	0.37
ref II	35036	3125	0.0	0.0	0.0	0.29
a	35490	3479	-3.9	10.8	0.26	0.30
b	36352	4151	-120.5	228.0	0.67	0.34
c	37233	4838	-47.8	50.3	0.98	0.32
d	38940	6170	46.2	95.8	2.25	0.38
d*	38940	6170	404.6	115.7	3.10	0.50

5. Conclusions

In this paper, the potential for integration of solar thermal power into a 1^{st} and 2^{nd} generation ethanol production process is studied by means of pinch analysis and multi-objective optimization. A solar field model was developed accounting for piping, storage, and energy conversion losses. The collector thermal output efficiency was determined according to a minute-by-minute time resolution solar model based on an actual product by Airlight Energy Holding SA [6].

It can be shown that adding 2^{nd} generation ethanol production to a 1^{st} generation plant can increase the product yield manifested in the carbon fixation rate by more than 25% ($C_{fix,\mathrm{refI}}$ = 0.22 vs

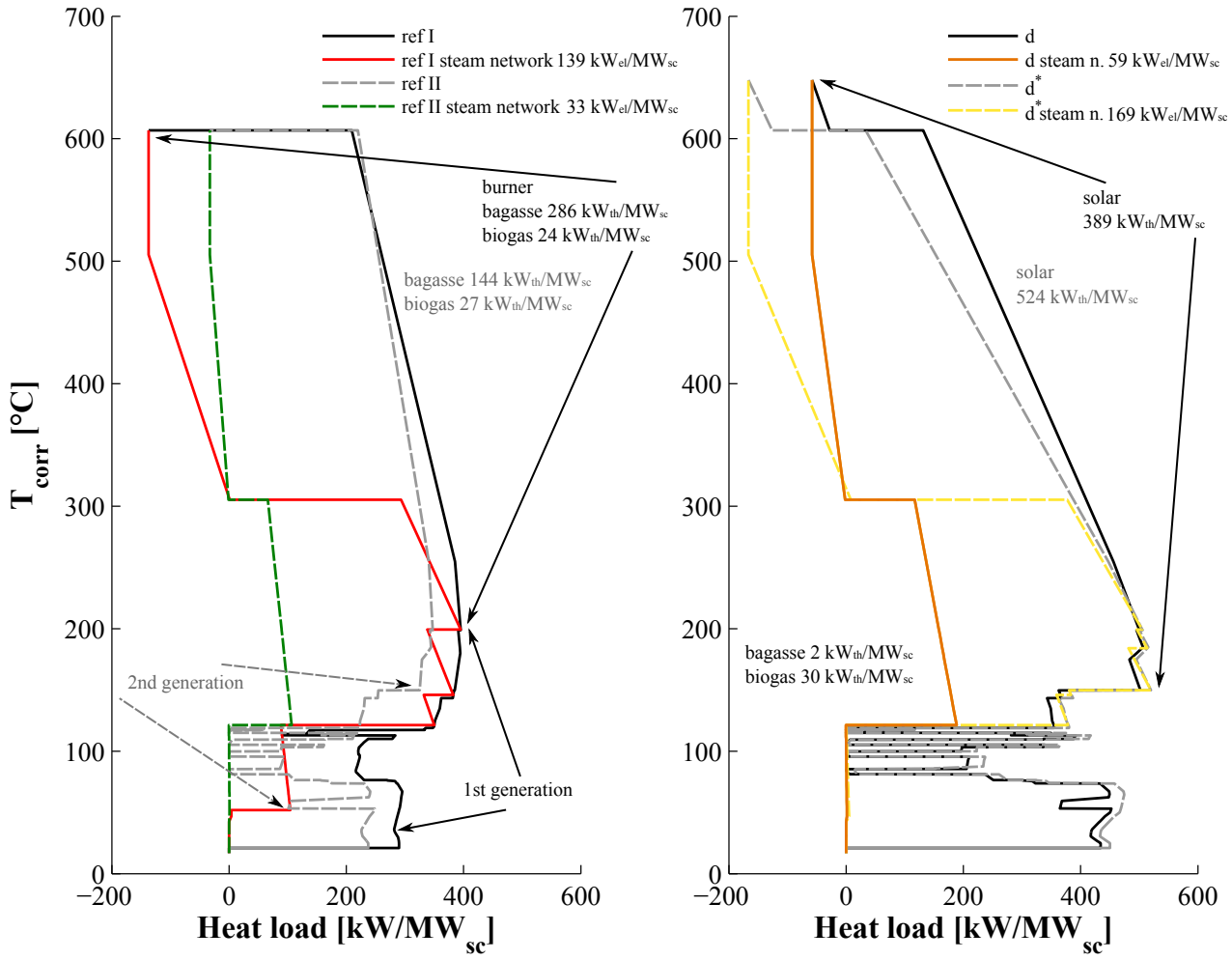

Fig. 9: Process and utitlity composite curves and respective steam network of ref I, ref II and solar integration scenario d and d (see Table 6). The leaves burner yields in every scenario a constant heat load of 177 kW_{th}/MW_{sc}.*

$C_{fix,\text{refII}} = 0.28$) for the same amount of biomass feedstock and plant surface area. Integration of solar heat can further improve the carbon fixation by round 20% ($C_{fix,\text{refII}} = 0.28$ vs $C_{fix,\text{d}} = 0.32$) for the same amount of biomass and surface area. This is related to a higher solar-to-thermal efficiency of the solar collectors (35%) as compared to biomass burning (<1%). The global efficiency can be increased by over 35% for the highest solar integration with respect to the 1^{st} generation ethanol production. The energy efficiency calculation might even underestimate the potential of the process, as the high-quality lignin resulting from the underlying process would not be used for energy production, but can be used in the chemical industry for the production of e.g. vanillin or other high-value chemicals. Therefore, integration of solar to the ethanol process has a threefold advantage: more product yield (carbon fixation) per surface area, a higher global efficiency and the exergy conservation of bagasse is increased, because it is transformed to ethanol and/or a high quality chemical product instead of heat. The penalizing factor remains the cost. The 2^{nd} generation ethanol production line is economically viable, but the current market situation for solar integration is not fully mature yet. However, further development of the technologies and economies of scale offer economic potential.
We conclude, that highly concentrated solar energy is a promising source for medium temperature process heat.

Acknowledgements

J. Albarelli acknowledges the financial support granted by CNPq (process 245662/2012-0).

Nomenclature

A_{coll}	[m]	collector active surface area
$A_{x,mean}$	[m^2]	mean area cross-section of main pipe in level x
b_{2g}	[-]	fraction of bagasse to 2^{nd} generation ethanol process
b_{2b}	[-]	fraction of bagasse to solar back-up burner
C_{fix}	[-]	percentage of carbon from fixed in the products
d_{al}	[m]	Aluminum layer thickness
d_{air}	[m]	air layer thickness
$d_{x,mean}$	[m]	mean diameter of main pipe in level x
f_a	[-]	correction factor for the finite length of the trough collector
f_{sm}	[-]	solar fraction; solar power at design conditions to the ethanol process
h_i	[kW/m^2K]	inner convective heat transfer coefficient
h_o	[kW/m^2K]	outside convective heat transfer coefficient
h_{wall}	[kW/m^2K]	overall pipe wall heat transfer coefficient
I_n	[kW/m^2]	direct normal incidence
k_{al}	[kW/mK]	thermal conductivity of aluminum
$k_{ht\ air}$	[kW/mK]	thermal conductivity of air (800 K)
k_n	[kW/mK]	thermal conductivity of pipe insulation layer n
LHV	[kJ/kg]	lower heating value
l_{coll}	[m]	solar collector length
l_x	[m]	solar field element length
$\dot{m}_{max,coll}$	[kW]	collector maximum air mass flow rate
$\dot{m}_x$	[kg/s]	mass flow rate leaving from level x
n	[-]	hour number
N_x	[-]	number of collectors on one branch of level x
N_{tot}	[-]	total number of collectors
p	[bar]	pressure inside the pipe
P_{coll}	[kW]	collector thermal power output
p_{stor}	[kW]	level position of storage in solar field
p_{sg}	[kW]	level position of steam generator in solar field
p_{rank}	[kW]	level position of Rankine cycle in solar field
$\dot{Q}_{th\ \text{air to ethanol process}}$	[kW]	thermal power delivered to ethanol process in the form of hot air
$\dot{Q}_{max,coll}$	[kW]	collector maximum power output
$\dot{Q}_{th\ \text{solar collector out, design}}$	[kW]	thermal power outlet from solar collectors
$\dot{Q}_{n,\ \text{stor}}$	[kW]	thermal power delivered to thermal storage
R	[J/Kkg]	mass based gas constant
r_i	[m]	pipe's inner radius
r_o	[m]	pipe's outer radius
$\dot{r}_{th\ \text{stor}}$	[kW]	actual rate at which the thermal storage is emptied or filled
sm	[-]	solar multiple; inverse of solar fraction
T_{ht}	[K]	hot temperature of the heat transfer fluid
$T_{ht\ air}$	[°C]	air collector outlet temperature
$T_{lt\ air}$	[°C]	air collector inlet temperature
$T_{ht\ steam}$	[°C]	steam generator outlet temperature
$T_{cond\ steam}$	[°C]	steam generator inlet temperature
$T_{lt\ steam}$	[°C]	Rankine outlet temperature
v_{ht}	[m/s]	high temperature velocity of heat transfer fluid
$v_{ht\ air}$	[m/s]	high temperature air velocity
$v_{ht\ steam}$	[m/s]	high temperature steam velocity
w_{coll}	[m]	solar collector width
w_1	[m]	minimum parallel collector spacing
w_x	[m]	solar field element width
$\Delta_{ht,pipe}$	[kW/m]	piping high temperature heat losses per surface area

Δ_{l}	[kW/m]	thermal losses per unit length of the receiver hot ducting
$\Delta_{\text{lt,pipe}}$	[kW/m]	piping low temperature heat losses per surface area
$\delta_{n,stor}$	[kW]	actual thermal storage content
δ_{ψ}	[-]	factor accounting for the tracking limits of the collector
η_{burner}	[-]	efficiency of back-up burner
η_{DNI}	[-]	collector yearly efficiency
η_{el}	[-]	electrical efficiency of solar field Rankine cycle
$\eta_{\text{el,off}}$	[-]	electrical efficiency of solar field Rankine cycle (off-season)
η_{GHI}	[-]	system global efficiency
η_{opt}	[-]	trough optical efficiency
η_{sg}	[-]	heat transfer efficiency of steam generator
η_{stor}	[-]	thermal storage efficiency
$\eta_{\text{Rank,th}}$	[-]	thermal efficiency of Rankine cycle
η_{th}	[-]	thermal efficiency of the receiver
ψ	[°]	collector tracking angle
θ_{skew}	[°]	skew angle, solar inlcination towards mirror surface

References

[1] C.A. Cardona Alzate and O.J. Sanchez Toro. Energy consumption analysis of integrated flowsheets for production of fuel ethanol from lignocellulosic biomass. *Energy*, 31(13):2447 – 2459, 2006.

[2] M.O.S. Dias, T.L. Junqueira, O. Cavalett, M.P. Cunha, C.D.F. Jesus, C.E.V. Rossell, R.M. Filho, and A. Bonomi. Integrated versus stand-alone second generation ethanol production from sugarcane bagasse and trash. *Bioresource Technology*, 103(1):152 – 161, 2012.

[3] A.V. Ensinas, V. Codina, F. Marechal, J.Q. Albarelli, and M.A. Silva. Thermo-economic optimization of integrated first and second generation sugarcane ethanol plant. *Chemical Engineering*, 35, 2013.

[4] A. Mian, A. Ensinas, G. Ambrosetti, and F. Maréchal. Optimal design of solar assisted hydrothermal gasification for microalgae to synthetic natural gas conversion. *Chemical Engineering Transactions*, 35, 2013.

[5] M.J. Montes, A. Abanades, J.M. Martinez-Val, and M. Valdes. Solar multiple optimization for a solar-only thermal power plant, using oil as heat transfer fluid in the parabolic trough collectors. *Solar Energy*, 83(12):2165 – 2176, 2009.

[6] Airlight Energy Holding SA. www.airlightenergy.ch. Accessed: 2013-01-14.

[7] S.A. Papoulias and I.E. Grossmann. A structural optimization approach in process synthesis i: Utility systems. *Computers & Chemical Engineering*, 7(6):695 – 706, 1983.

[8] S.A. Papoulias and I.E. Grossmann. A structural optimization approach in process synthesis ii: Heat recovery networks. *Computers & Chemical Engineering*, 7(6):707 – 721, 1983.

[9] S.A. Papoulias and I.E. Grossmann. A structural optimization approach in process synthesis iii: Total processing systems. *Computers & Chemical Engineering*, 7(6):723 – 734, 1983.

[10] F. Marechal and B. Kalitventzeff. Process integration: Selection of the optimal utility system. *Computers & Chemical Engineering*, 22, Supplement 1(0):S149 – S156, 1998.

[11] G.D. Ulrich. *Chemical Engineering - Process Design and Economics A Practical Guide*. Process Publishing, Durham, NH, USA, 2nd edition, 2004.

[12] R. Turton, W. Whiting, and J. Shaeiwitz. *Analysis, Synthesis and Design of Chemical Processes*. Prentice-Hall, 3rd edition, 2009.

[13] Aspen Technology Inc. www.aspentech.com. Accessed: 2013-01-14.

[14] Raffaele Bollinger. *Méthodologie de la synthèse des systèmes énergétiques Industriels*. PhD thesis, Ecole Politechnique Fédérale de Lausanne, Switzerland, 2010.

[15] Meteonorm 7.0. Technical report, METEOTEST, www.meteonorm.com. Accessed 2013-01-14.

[16] SolarGIS iMaps ©2014 GeoModel Solar. http://solargis.info/doc/48. Accessed: 2013-01-14.

[17] Ibrahim Reda and Afshin Andreas. Solar position algorithm for solar radiation applications. *Solar Energy*, 76(5):577 – 589, 2004. http://rredc.nrel.gov/solar/codesandalgorithms/spa/.

[18] DIY Trade - global trading platform. http://www.diytrade.com/china/pd/2607205/. Large_Diameter_Spiral_SAW_Steel_Pipe.html, Accessed: 2013-01-14.

[19] G. Zanganeh, A. Pedretti, S. Zavattoni, M. Barbato, and A. Steinfeld. Packed-bed thermal storage for concentrated solar power - pilot-scale demonstration and industrial- scale design. *Solar Energy*, 86(10):3084 – 3098, 2012.

[20] Germain Augsburger. *Thermo-Economic Optimization of Large Solar Tower Power Plants*. PhD thesis, Ecole Polytechnique de Lausanne, 2013.

[21] Hans W. Fricker. High-temperature heat storage using natural rock. *Solar Energy Materials*, 24(14):249 – 254, 1991.

[22] U. Langnickel, A. Steinfeld, J. Karni, E. Zarza, and O. Popel. Development steps for parabolic trough solar power technologies with maximum impact on cost reduction. *Journal of Solar Energy Engineering*, 129(4):371, 2007.

[23] Stephen Hall. *Rules of Thumb for Chemical Engineers*. Butterworth-Heinemann (Elsevier Inc), 5th edition, 2012.

[24] J.Q. Albarelli, A.V. Ensinas, and M.A. Silva. Product diversification to enhance economic viability of second generation ethanol production in brazil: The case of the sugar and ethanol joint production. *Chemical Engineering Research and Design*, (0):–, 2013.

[25] X. Pan, N. Gilkesand J. Kadla, K. Pye, S. Saka, D. Gregg, K. Ehara, D. Xie, and D. Lamand J.Saddler. Bioconversion of hybrid poplar to ethanol and co-products using an organosolv fractionation process: Optimization of process yields. *Biotechnology and Bioengineering*, 94(5):851–861, 2006.

[26] V. Arantes and J.N. Saddler. Cellulose accessibility limits the effectiveness of minimum cellulase loading on the efficient hydrolysis of pretreated lignocellulosic substrates. *Biotechnology for Biofuels*, 4(1):1–17, 2011.

[27] Preco-teto de leilao de energia desencoraja investimentos em bioeletricidade. http://www.unica.com. Accessed: 2013-01-14.

[28] N. Smolarski. High-value opportunities for lignin: unlocking its potential. *Frost & Sullivan*, 2012.

[29] M.O.S. Dias, M.P. Cunha, R.F. Maciel, A. Bonomi, C.D.F. Jesus, and C.E.V. Rossell. Simulation of integrated first and second generation bioethanol production from sugarcane: comparison between different biomass pretreatment methods. *Journal of Industrial Microbiology & Biotechnology*, 38(8):955–966, 2011.